

Structural Analysis of Species in NbCl₅-EMIC Room-Temperature Molten Salt with Raman Spectroscopic Measurement and *Ab Initio* Molecular Orbital Calculation

Nobuyuki Koura*, Hidenori Matsuzawa[†], Tomoki Kato*, Yasushi Idemoto*, and Futoshi Matsumoto*

Faculty of Engineering, Chiba Institute of Technology, 2-1-1 Shibazono, Narashino, Chiba 275-0023, Japan

*Faculty of Science and Technology, Tokyo University of Science, 2641 Yamazaki, Noda, Chiba 278-8510, Japan

(Received June 22, 2002 : Accepted October 8, 2002)

Abstract. The structure of species formed in NbCl₅-1-ethyl-3-methylimidazolium chloride (EMIC) room-temperature molten salt (RTMS) was examined with the Raman spectroscopic measurement and *ab initio* molecular orbital calculation. The equilibrium structures of NbCl₅, NbCl₆⁻, Nb₂Cl₁₀, Nb₂Cl₁₁⁻, Nb₃Cl₁₆⁻, NbCl₆⁻-EMI⁺ (in which NbCl₆⁻ anion approaches EMI⁺ cation with strong interaction) and Nb₂Cl₁₁⁻-EMI⁺ were obtained with the HF/LANL2DZ level of calculation. The harmonic frequencies at each equilibrium structure were compared with Raman spectra. The harmonic frequencies of NbCl₆⁻-EMI⁺, Nb₂Cl₁₁⁻-EMI⁺, and Nb₂Cl₁₀ were in good agreement with the Raman spectra of RTMS melts. In the NbCl₅-EMIC RTMS, the main species were NbCl₆⁻ and EMI⁺. In the NbCl₅-EMIC RTMS added NbCl₅ over 50 mol%, small amount of Nb₂Cl₁₁⁻ and Nb₂Cl₁₀ were also formed. The structures of anions and cation in the RTMS distorted from free ions with Coulomb force.

Key words: Room-temperature molten salt, Raman spectra, *Ab initio* molecular orbital calculation, EMIC

1. Introduction

Room-temperature molten salts (RTMS) have several unique properties, such as a wide electrochemical window, high inherent conductivity, negligible vapor pressure, and nonflammability¹⁻³). The commonly known application of RTMS is the electrodeposition of metal and alloy from the RTMS. The electrodeposition of alloys, such as amorphous Ni-Zn⁴) and Co-Zn⁵), Nb₃Sn superconductor⁶), and the control of crystal orientation of the deposit obtained from the RTMS⁷) has been reported. Moreover, many useful electrochemical depositions for industry, which does not occur in aqueous and organic solutions, have also been found in the RTMS⁸⁻¹⁰). Although characteristics of electrochemical depositions in the RTMS originate mainly from the extension of potential windows, we consider that the molecular structure of species in the RTMS and the relative position of species to other species contribute to the characteristics of the deposit obtained from the RTMS.

In this study, the structure of species formed in NbCl₅-EMIC RTMS and the interaction between species are examined with *ab initio* molecular orbital calculation and the Raman spectra. The structure and the surrounding of the species in various compositions (various ratios of NbCl₅ and EMIC) of the RTMS are identified. The structure and relative position of species to other species are discussed in detail. The NbCl₅-EMIC RTMS is a constituent of NbCl₅-SnCl₂-

EMIC RTMS, from which the Nb₃Sn superconductor is deposited electrochemically⁶). In the elucidation of the structure of NbCl₅-SnCl₂-EMIC RTMS, the analysis of the structure of NbCl₅-EMIC RTMS is the first step.

2. Experimental

2.1. Preparation of the RTMS and Raman spectroscopic measurement

EMIC was synthesized based on the previous report¹¹). NbCl₅ (Wako Pure Chemical Industries, Ltd., Japan) is used without further purification. NbCl₅-EMIC RTMS was prepared by the addition of NbCl₅ to EMIC with stirring at 130°C. After the addition of NbCl₅, the melt was stirred at 130°C for 24 h under an atmosphere of argon. Five samples of NbCl₅ (33 mol%)-EMIC (67 mol%) RTMS (33/67 melt), 48/52, 52/48, 60/40, and 67/33 melts, sealed crystal tube and chilled by liquid nitrogen, were used for Raman spectroscopic measurement. Raman spectra were measured by a laser Raman spectrometer (NRS-2000, JASCO, Japan) equipped with an optical multichannel analyzer. The 514.5 nm line from an argon ion laser was used for excitation. The spectra were taken by 10 accumulations during 30 second exposures (2 cm⁻¹ resolution).

2.2. Calculation method.

The calculations were carried out at the Hartree-Fock (HF) method with the LANL2DZ basis set^{11,13}) by using the GAUSSIAN 98 program package¹⁴) on a Fujitsu VPP5000/3

[†]E-mail: matuzawa@pf.it-chiba.ac.jp

and a IBM RS/600 SP at Tokyo University of Science and a NEC HPC at Institute for Molecular Science (IMS). The geometries of the free NbCl_5 , NbCl_6^- , $\text{Nb}_2\text{Cl}_{10}$, $\text{Nb}_2\text{Cl}_{11}^-$, $\text{Nb}_3\text{Cl}_{16}^-$ and EMI^+ were optimized at first. Then NbCl_6^- - EMI^+ and $\text{Nb}_2\text{Cl}_{11}^-$ - EMI^+ structures were optimized. In order to find the most stable orientation of anion and cation pair in each NbCl_6^- - EMI^+ and $\text{Nb}_2\text{Cl}_{11}^-$ - EMI^+ system, the geometry optimizations of the possible configurations of anion species around EMI^+ were carried out. The harmonic vibrational frequencies at each optimized geometry were calculated for the comparison of the Raman spectra and the evaluation of the stability of optimized geometries.

3. Results and Discussion

3.1. Raman spectra of NbCl_5 -EMIC RTMS

Raman spectra for NbCl_5 (33 mol%)-EMIC (67 mol%) RTMS (33/67 melt), 48/52, 52/48, 60/40 and 67/33 melts have been obtained. These spectra are presented in Fig. 1. A strong band at 371 cm^{-1} and two weak bands at 324 and 288 cm^{-1} are found in the spectra of all RTMS melts. Two bands at 192 and 172 cm^{-1} of 60/40 and 67/33 melts are recognized to be a broad band about 180 cm^{-1} of 33/67, 48/52 and 52/48 melts because of low resolution. In the RTMS added NbCl_5 over 52 mol%, bands at 419 and 393 cm^{-1} appear with an increase of the amount of NbCl_5 added in the NbCl_5 -EMIC RTMS. The intensity of the bands at 393 cm^{-1} of both 60/40

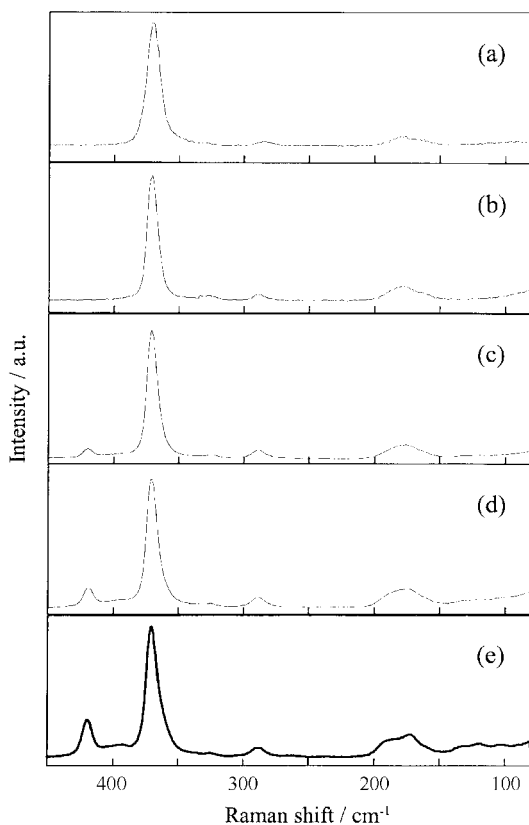
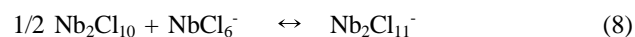


Fig. 1. Raman spectra of NbCl_5 -EMIC RTMS. (a) 33/67, (b) 48/52, (c) 52/48, (d) 60/40, and (e) 67/33 melts.

and 67/33 melts is very weak. These results indicate that the new species are produced in the NbCl_5 -EMIC RTMS added NbCl_5 over 50 mol%, including the species of which bands appeared at 371 , 324 , 288 and about 180 cm^{-1} . It is well known that equilibria between the species are established in the RTMS composed of metal halides and alkyipyridinium halides¹⁵ or di-alkylimidazolium halides¹¹. Various species are also formed depending on the mixing ratio of the metal halides and alkyipyridinium halides or di-alkylimidazolium halides. For example, equilibria between the species in the AlCl_3 -EMIC RTMS are commonly described as follows:^{11,16}



The major species is AlCl_4^- for basic melts (< 50 mol% AlCl_3), and Al_2Cl_7^- for acidic melts (> 50 mol% AlCl_3). In CuCl -1-butylpyridinium chloride (BPC)¹⁵ and SnCl_2 -BPC RTMS¹⁷, similar equilibria have been also established. We also postulate similar equilibria (eqs. (1) and (6-9)) for the NbCl_5 -EMIC RTMS as follows:



Based on these equilibria, it is assumed that NbCl_5 and NbCl_6^- species exist in all the RTMS, and $\text{Nb}_2\text{Cl}_{10}$, $\text{Nb}_2\text{Cl}_{11}^-$, and $\text{Nb}_3\text{Cl}_{16}^-$ species are formed with an increase in the amount of added NbCl_5 . The strong band at 371 cm^{-1} and several weak bands observed in Fig. 1(a, b) originate from the NbCl_5 and / or NbCl_6^- species. Bands at 393 and 419 cm^{-1} originated from the $\text{Nb}_2\text{Cl}_{10}$, $\text{Nb}_2\text{Cl}_{11}^-$, and/or $\text{Nb}_3\text{Cl}_{16}^-$ species.

3.2. Equilibrium structure

Figure 2 shows the equilibrium structures of NbCl_5 (a), NbCl_6^- (b), $\text{Nb}_2\text{Cl}_{10}$ (c), $\text{Nb}_2\text{Cl}_{11}^-$ (d) and $\text{Nb}_3\text{Cl}_{16}^-$ (e) with some bond lengths and angles. The stable structures of NbCl_5 and NbCl_6^- with HF/LANL2DZ level are in agreement with those of the CASSCF level of calculation by Rosenkilde, et al¹⁸. The symmetries of NbCl_5 and NbCl_6^- are D_{3h} and O_h , respectively. The axial and equatorial Nb-Cl bond lengths for NbCl_5 are different. On the other hand, the bond lengths of all Nb-Cl in NbCl_6^- show the same value (2.42 \AA). In the stable structure of $\text{Nb}_2\text{Cl}_{10}$ (C_{2v} symmetry), two Nb(V) ions, two Cl^- ions bridging Nb(V) ions and four Cl^- ions binding to Nb(V) ions lie in a plane. In the case of $\text{Nb}_2\text{Cl}_{11}^-$ and $\text{Nb}_3\text{Cl}_{16}^-$, Nb(V) ions are bridged through a Cl^- . Two stable

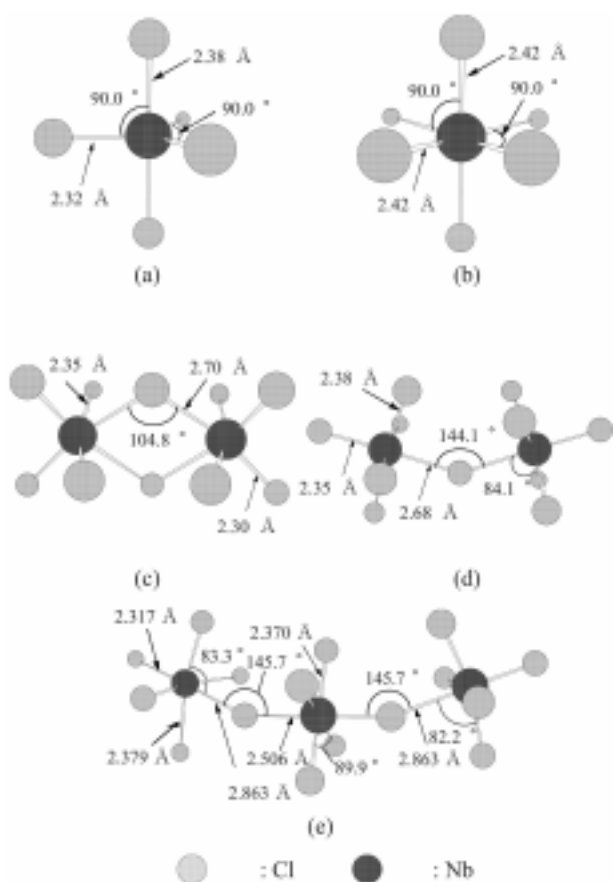


Fig. 2. Equilibrium structures of (a) NbCl_5 , (b) NbCl_6^- , (c) $\text{Nb}_2\text{Cl}_{10}$, (d) $\text{Nb}_2\text{Cl}_{11}^-$, and (e) $\text{Nb}_3\text{Cl}_{16}^-$.

structures of $\text{NbCl}_6^- \text{-EMI}^+$ with some bond lengths and angles are shown in Fig. 3. There is no difference of stabilization energy between $\text{NbCl}_6^- \text{-EMI}^+$ (I) and $\text{NbCl}_6^- \text{-EMI}^+$ (II) ($\text{NbCl}_6^- \text{-EMI}^+$ (I): 274 kJ/mol and $\text{NbCl}_6^- \text{-EMI}^+$ (II): 272 kJ/

mol). From the values of the stabilization energies, it is found that NbCl_6^- and EMI^+ are interacted by strong Coulomb force. No transition state between two local minima, (I) and (II), is found on the potential energy surface, because the same total energy is obtained with the single point calculations of several geometries between (I) and (II). By all of the geometry optimization of $\text{NbCl}_6^- \text{-EMI}^+$, the stable structure of (I) or (II) is obtained according to the initial geometry. The Nb-Cl bond lengths and Cl-Nb-Cl angles are slightly changed by the interaction between NbCl_6^- and EMI^+ .

By the geometry optimizations of $\text{Nb}_2\text{Cl}_{11}^- \text{-EMI}^+$, two stable structures, $\text{Nb}_2\text{Cl}_{11}^- \text{-EMI}^+$ (I) and $\text{Nb}_2\text{Cl}_{11}^- \text{-EMI}^+$ (II) are obtained as well as $\text{NbCl}_6^- \text{-EMI}^+$. Figure 4 shows two stable structures of $\text{Nb}_2\text{Cl}_{11}^- \text{-EMI}^+$ with some bond lengths and angles. The stabilization energies of 272 kJ/mol (I) and 265 kJ/mol (II) are the same essentially. There is no transition state between (I) and (II). The $\text{Nb}_2\text{Cl}_{11}^-$ is slightly distorted by the Coulomb interaction with EMI^+ .

In the $\text{NbCl}_5 \text{-EMIC}$ RTMS, there are two local structures of each $\text{NbCl}_6^- \text{-EMI}^+$ and $\text{Nb}_2\text{Cl}_{11}^- \text{-EMI}^+$ based on Coulomb interaction. Furthermore, in the equilibrium geometries both $\text{NbCl}_6^- \text{-EMI}^+$ and $\text{Nb}_2\text{Cl}_{11}^- \text{-EMI}^+$, common characteristics about the relation between anion and cation are found. The positive charge of the hydrogen attracted Cl atom is included from +0.19 (free EMI^+) to +0.34 by forming $\text{NbCl}_6^- \text{-EMI}^+$ or $\text{Nb}_2\text{Cl}_{11}^- \text{-EMI}^+$. This value is the largest of all elements in EMI^+ with NbCl_6^- or $\text{Nb}_2\text{Cl}_{11}^-$. Mulliken charges of other hydrogen atoms in EMI^+ show +0.20 - +0.26 region and slightly changed by the ion pair formation. One of carbon atom (2nd position) in imidazolium ring has also positive charge (+0.21) though other atoms of imidazolium ring have negative charges. On the other hand, in $\text{EMI}^+ \text{-NbCl}_6^-$ (I) and (II), the negative charges (-0.32) of three Cl atoms near EMI^+ are larger than those (-0.18) of other Cl atoms. The negative charges of three Cl atoms are increased by the contact

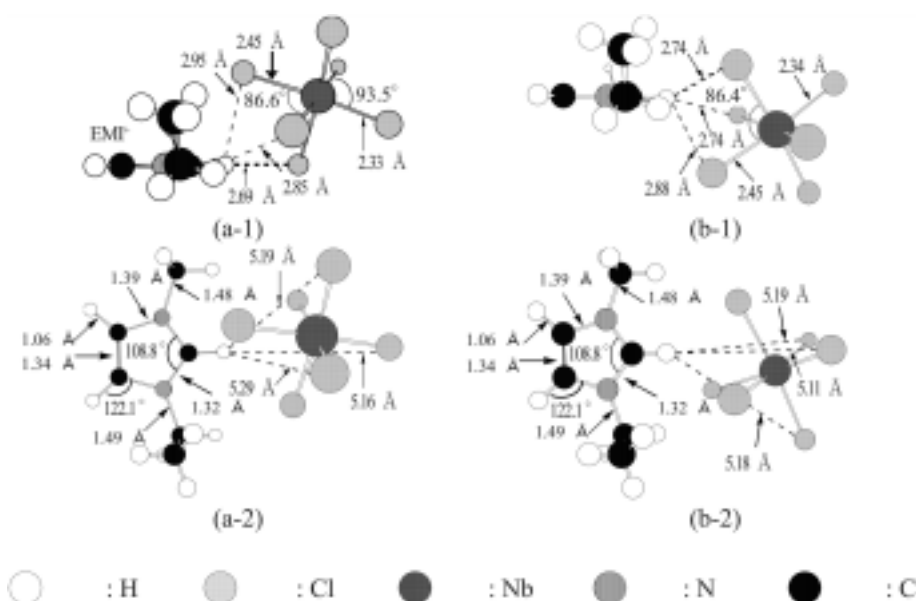


Fig. 3. Equilibrium structures of (a) $\text{NbCl}_6^- \text{-EMI}^+$ (I), (b) $\text{NbCl}_6^- \text{-EMI}^+$ (II). Each structure is shown from the side (1) and top(2) views.

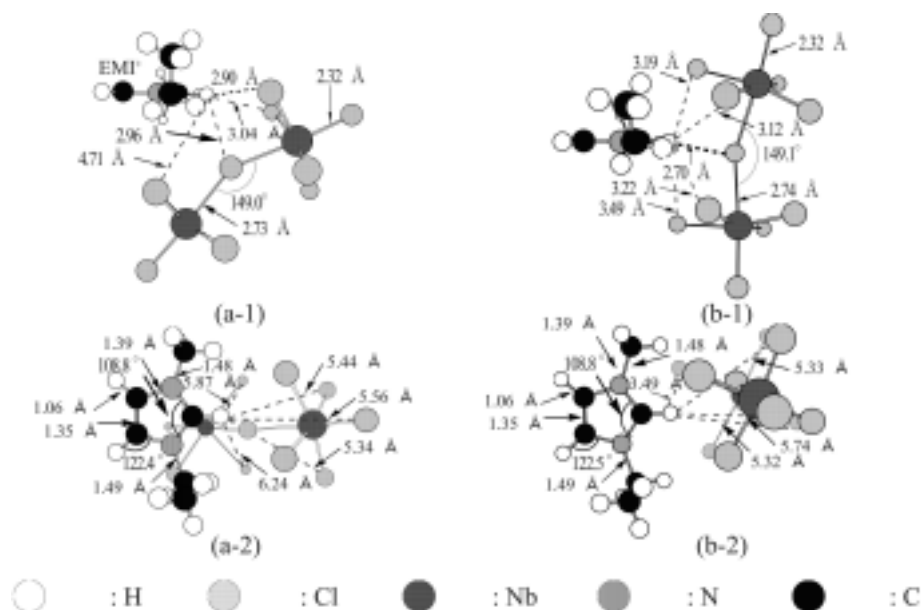


Fig. 4. Equilibrium structures of (a) $\text{Nb}_2\text{Cl}_{11}^- \text{EMI}^+$ (I), and (b) $\text{Nb}_2\text{Cl}_{11}^- \text{EMI}^+$ (II). Each structure is shown from the side (1) and top (2) views.

with EMI^+ (from -0.27 to -0.32). On the other hand, the negative charges of Cl atoms located outside the contact with EMI^+ are decreased from -0.27 to -0.18 e^- . In the case of $\text{EMI}^+ - \text{Nb}_2\text{Cl}_{11}^-$, (I) and (II), one Cl atom bridged two NbCl_5 units has large negative charge (-0.34). This negative charge is increased from -0.29 to -0.34 by the ion pair formation with EMI^+ . Mulliken charges of other Cl atoms show -0.17 - -0.26 region. Sum of Mulliken charges of NbCl_6^- and $\text{Nb}_2\text{Cl}_{11}^-$ is -0.95 and -0.78, respectively. Therefore, Cl atoms closed to EMI^+ in NbCl_6^- and $\text{Nb}_2\text{Cl}_{11}^-$ mainly approaches to a hydrogen atom connected to carbon atom (2nd position) from the upper or lower side of imidazolium ring by Coulomb force, and small charge transfer from anion to cation is also found. The approach of NbCl_6^- or $\text{Nb}_2\text{Cl}_{11}^-$ to the hydrogen from the direction parallel to the imidazolium ring might be blocked by the steric hindrance between methyl or ethyl groups because NbCl_6^- and $\text{Nb}_2\text{Cl}_{11}^-$ have large molecular sizes.

3.3. Comparison of observed and calculated Raman spectra

Figure 5 shows the observed Raman spectra and calculated harmonic vibrational frequencies showing the Raman activation. Two observed Raman spectra, (a) and (b), are obtained in 33/67 and 67/33 melts, respectively. The harmonic vibrational frequencies of (c), (d), (e), (f) and (g) are calculated at the equilibrium structures of free NbCl_5 , NbCl_6^- , $\text{Nb}_2\text{Cl}_{10}$, $\text{Nb}_2\text{Cl}_{11}^-$ and $\text{Nb}_3\text{Cl}_{16}^-$, respectively, without scaling. There is no strong band in the frequency analysis of EMI^+ . The experimental results of Raman spectra for NbCl_5 -EMIC RTMS have been already discussed. In this section, the calculated vibrational frequencies are compared with the experimental.

The calculated frequencies at 188(E''), 290(A_1') and 382(A_1') cm^{-1} of NbCl_5 are assigned to degenerate Cl-Nb-Cl bending, Cl-Nb stretching and Cl-Nb stretching modes,

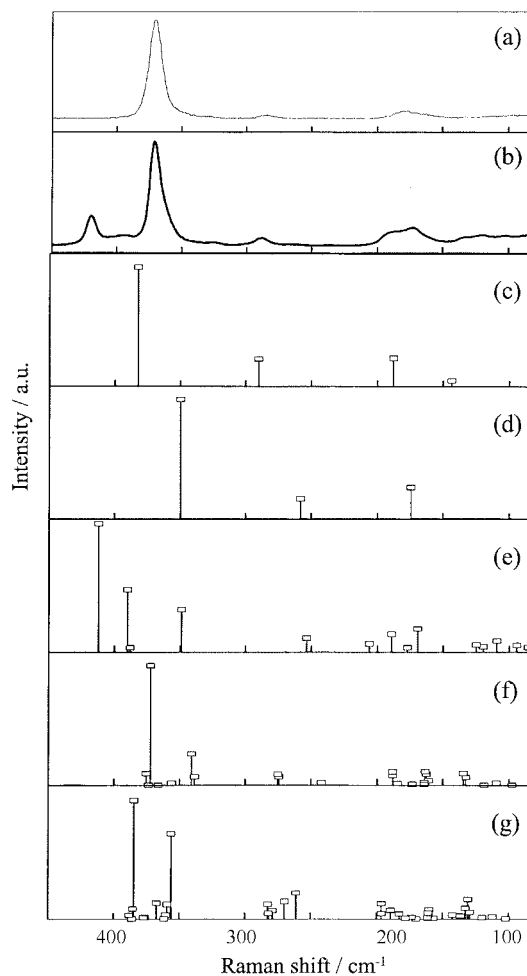


Fig. 5. Comparison between the Raman spectra in (a) 33/67 and (b) 67/33 melts and calculated vibrational frequencies at the equilibrium structures of (c) NbCl_5 , (d) NbCl_6^- , (e) $\text{Nb}_2\text{Cl}_{10}$, (f) $\text{Nb}_2\text{Cl}_{11}^-$, and (g) $\text{Nb}_3\text{Cl}_{16}^-$.

respectively. As the band at 382 cm^{-1} is higher frequency than that of 33/67 (a) and 67/33 (b) melts (371 cm^{-1}), NbCl_5 as a species in RTMS is not confirmed.

By the frequency analysis of free NbCl_6^- , the harmonic vibrational frequencies of $174\text{ (T}_{2g}\text{)}$, $258\text{ (E}_g\text{)}$ and $350\text{ (A}_{1g}\text{)}$ cm^{-1} are obtained (Fig. 5(d)). These frequencies are in good agreement with the Raman spectra of 33/67 melt when they are shifted to $20\text{--}30\text{ cm}^{-1}$ higher frequencies. We assume that these frequencies of free NbCl_6^- are shifted by the interaction with EMI^+ .

The harmonic frequencies at two equilibrium structures, (I) and (II), of $\text{NbCl}_6^- \text{--EMI}^+$ are shown in Figure 6. The calculated frequencies of $\text{NbCl}_6^- \text{--EMI}^+$ (I) are approximately similar to those of $\text{NbCl}_6^- \text{--EMI}^+$ (II). The frequencies at 174 and 258 cm^{-1} assigned to degenerate Cl-Nb-Cl bending and Cl-Nb stretching modes, respectively, of free NbCl_6^- (Fig. 5(d)) shift to around 176 and 250 cm^{-1} , respectively, and they are split in some peaks by forming the ion pair with EMI^+ . The band at 350 cm^{-1} of free NbCl_6^- shifts to 369 cm^{-1} of $\text{NbCl}_6^- \text{--EMI}^+$. The band at 327 cm^{-1} assigned to Cl-Nb stretching mode is appeared newly by forming ion pair of NbCl_6^- and EMI^+ . These calculated frequencies of $\text{NbCl}_6^- \text{--EMI}^+$ except 250 cm^{-1} are in good agreement with the observed Raman spectra of 33/67 and 67/33 melts (180 , 324 and 371 cm^{-1}). The calculated frequencies at around 250 cm^{-1} might be corresponded to the broad band at 288 cm^{-1} in Raman spectra of 33/67 and 67/33 melts.

The calculated harmonic vibrational frequencies of $\text{Nb}_2\text{Cl}_{10}$ are shown in Fig. 5(e). Three large peaks of $349\text{ (A}_1\text{)}$, $390\text{ (B}_2\text{)}$ and $412\text{ (A}_1\text{)}$ cm^{-1} assigned to Cl-Nb-Cl bending, Cl-Nb stretching and Cl-Nb stretching, respectively, are compared with the experimental. The peak at 412 cm^{-1} is close to the band at 419 cm^{-1} of 67/33 melt. Bues, et al., have been reported that Raman spectrum of $\text{Nb}_2\text{Cl}_{10}$ appears at 419 cm^{-1} ¹⁹⁾. As the $\text{Nb}_2\text{Cl}_{10}$ is not ion pair with EMI^+ but independent species, the band at 419 cm^{-1} in the Raman spectra is assigned to $\text{Nb}_2\text{Cl}_{10}$.

In the theoretical Raman spectra of free $\text{Nb}_2\text{Cl}_{11}^-$ (Fig. 5(f)), a strong peak appears at 372 cm^{-1} . In RTMS melt, there is no free $\text{Nb}_2\text{Cl}_{11}^-$, though this peak is close to the strong band at 371 cm^{-1} in 33/67 and 67/33 melts. The frequency analysis of $\text{Nb}_2\text{Cl}_{11}^- \text{--EMI}^+$ system is required because this anion is able to interact with EMI^+ strongly, as well as $\text{NbCl}_6^- \text{--EMI}^+$ system. The calculated harmonic vibrational frequencies of $\text{Nb}_2\text{Cl}_{11}^- \text{--EMI}^+$ (I) and (II) systems are shown in Fig. 6(e) and (f), respectively. The frequency of the strong peak at 392 cm^{-1} is in good agreement with the broad weak band at 393 cm^{-1} in 67/33 melt. The band at 393 cm^{-1} is assigned to $\text{Nb}_2\text{Cl}_{11}^-$ interacted with EMI^+ . In the Raman spectra of the melts, the intensity of 393 cm^{-1} is smaller than that of the strongest peak of 371 cm^{-1} assigned to NbCl_6^- . This intensity means that amount of $\text{Nb}_2\text{Cl}_{11}^-$ is less than that of NbCl_6^- .

In the frequency analysis of free $\text{Nb}_3\text{Cl}_{16}^-$, two strong peaks at 356 and 385 cm^{-1} are obtained (Fig. 5(g)). It is considered that the amount of $\text{Nb}_3\text{Cl}_{16}^-$ is less than that of $\text{Nb}_2\text{Cl}_{11}^-$ when the RTMS melt contains $\text{Nb}_3\text{Cl}_{16}^-$ based on

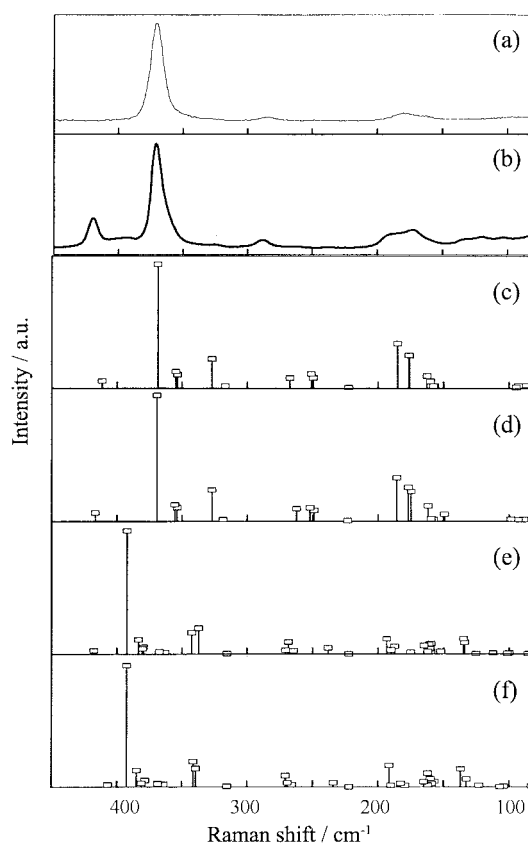


Fig. 6. Comparison between the Raman spectra in (a) 33/67 and (b) 67/33 melts and the calculated vibrational frequencies at the equilibrium structures of (c) $\text{NbCl}_6^- \text{--EMI}^+$ (I), (d) $\text{NbCl}_6^- \text{--EMI}^+$ (II), (e) $\text{Nb}_2\text{Cl}_{11}^- \text{--EMI}^+$ (I), and (f) $\text{Nb}_2\text{Cl}_{11}^- \text{--EMI}^+$.

eqs. (8) and (9). Furthermore, the frequency analysis of $\text{Nb}_3\text{Cl}_{16}^- \text{--EMI}^+$ system is required for the confirmation of $\text{Nb}_3\text{Cl}_{16}^-$ as the component species of melts. However, we are not able to obtain the optimized geometry and harmonic vibrational frequencies of $\text{Nb}_3\text{Cl}_{16}^- \text{--EMI}^+$ system because of the computational limit.

From the comparison between calculated harmonic frequencies of all examined species and Raman spectra of 33/67 melts, it is found that only NbCl_6^- ion interacted with EMI^+ is containing in the $\text{NbCl}_5\text{--EMIC}$ RTMS added below 50 mol% NbCl_5 . In Fig. 6(b), the band at 419 cm^{-1} is assigned to $\text{Nb}_2\text{Cl}_{10}$ from both experimental and theoretical results. Broad band at 393 cm^{-1} is assigned to $\text{Nb}_2\text{Cl}_{11}^-$ with EMI^+ . The strongest peak at 371 cm^{-1} is assigned to NbCl_6^- with EMI^+ . Therefore, in the $\text{NbCl}_5\text{--EMIC}$ RTMS added over 50 mol% NbCl_5 , it is found that NbCl_6^- , $\text{Nb}_2\text{Cl}_{10}$ and $\text{Nb}_2\text{Cl}_{11}^-$ are containing, by the comparison between calculated harmonic frequencies and Raman spectra of 67/33 melts. From both Raman spectra and theoretical approach, we cannot confirm that there is $\text{Nb}_3\text{Cl}_{16}^-$ in 67/33 melts. Both NbCl_6^- and $\text{Nb}_2\text{Cl}_{11}^-$ ions interact with EMI^+ in RTMS. Certainly, two species, $\text{Nb}_2\text{Cl}_{10}$ and $\text{Nb}_2\text{Cl}_{11}^-$, are formed according to the reactions of eqs. (6) and (8), respectively. The Raman intensities of 67/33 melt suggest that the amounts of $\text{Nb}_2\text{Cl}_{10}$ and $\text{Nb}_2\text{Cl}_{11}^-$ are small in 67/33 melt.

4. Conclusion

The stable structures of NbCl_5 , NbCl_6^- , $\text{Nb}_2\text{Cl}_{10}$, $\text{Nb}_2\text{Cl}_{11}^-$, $\text{Nb}_3\text{Cl}_{16}^-$, $\text{NbCl}_6^- \text{-EMI}^+$ and $\text{Nb}_2\text{Cl}_{11}^- \text{-EMI}^+$ as the chemical species in NbCl_5 -EMIC RTMS were obtained with ab initio molecular orbital calculation. The stabilization energies of $\text{NbCl}_6^- \text{-EMI}^+$ and $\text{Nb}_2\text{Cl}_{11}^- \text{-EMI}^+$ suggested that the anions interacted with EMI^+ by strong Coulomb force. The harmonic frequencies at the equilibrium geometries of all examined species were compared with Raman spectra of 33/67 and 67/33 melts. Raman spectra of 33/67 melt were in good agreement with the calculated harmonic frequencies of $\text{NbCl}_6^- \text{-EMI}^+$ system. The peaks of other species was not containing in Raman spectra of 33/67 melt. From the comparison between Raman spectra of 67/33 melt and calculated harmonic frequencies of all examined species, it was found that three species, NbCl_6^- , $\text{Nb}_2\text{Cl}_{10}$, $\text{Nb}_2\text{Cl}_{11}^-$, are containing in 67/33 melt. Both NbCl_6^- and $\text{Nb}_2\text{Cl}_{11}^-$ are interacted with EMI^+ in 67/33 melt.

References

1. C. S-Kelley and R. T. Carline, *J. Electrochem. Soc.*, **141**, 873 (1994).
2. J. Fuller, R. A. Osteryoung, and R. T. Carlin, *J. Electrochem. Soc.*, **142**, 3632 (1995).
3. N. Koura, K. Iizuka, Y. Idemoto, and K. Ui, *Electrochemistry*, **67**, 706 (1999).
4. N. Koura, Y. Suzuki, Y. Idemoto, and F. Matsumoto, *Hyomen Gijutsu*, **52**, 116 (2001).
5. N. Koura, Y. Idemoto, and T. Matsumoto, *Hyomen Gijutsu*, **49**, 1215 (1998).
6. N. Koura, K. Shibano, F. Matsumoto, H. Matsuzawa, T. Katou, and Y. Idemoto, *Hyomen Gijutsu* **52**, 645 (2001).
7. N. Koura, F. Matsumoto, Y. Tashiro, M. Futamura, and Y. Idemoto, *Hyomen Gijutsu*, **52**, 791 (2001).
8. M. K. Carpenter, *J. Mater. Res.*, **9**, 2584 (1994).
9. M. K. Carpenter and M. Verbrugge, *J. Electrochem. Soc.*, **137**, 123 (1990).
10. Y. S. Fung and W. B. Zhang, *J. Appl. Electrochem.*, **27**, 857 (1997).
11. J. S. Wilkes, J. A. Levisky, R. A. Wilson, and C. L. Hussey, *Inorg. Chem.*, **21**, 1263 (1982).
12. P. J. Hay and W. R. Wadt, *J. Chem. Phys.*, **82**, 270 (1985).
13. W. R. Wadt and P. J. Hay, *J. Chem. Phys.*, **82**, 284 (1985).
14. Gaussian 98, Revision A.9, M. J. Frisch, G. W. Trucks, H. B. Schlegel, G. E. Ecuseria, M. A. Robb, J. R. Cheeseman, V. G. Zakrzewski, J. A. Montgomery, Jr., R. E. Stratmann, J. C. Burant, S. Dapprich, J. M. Millam, A. D. Daniels, K. N. Kudin, M. C. Strain, O. Farkas, J. Tomasi, V. Barone, M. Cossi, R. Cammi, B. Mennucci, C. Pomelli, C. Adamo, S. Clifford, J. Ochterski, G. A. Petersson, P. Y. Ayala, Q. Cui, K. Morokuma, D. K. Malick, A. D. Rabuck, K. Raghavachari, J. B. Foresman, J. Cioslowski, J. V. Ortiz, A. G. Baboul, B. B. Stefanov, G. Liu, A. Liashenko, P. Piskorz, I. Komaromi, R. Gomperts, R. L. Martin, D. J. Fox, T. Keith, M. A. Al-Laham, C. Y. Peng, A. Nanayakkara, M. Challacombe, P. M. W. Gill, B. Johnson, W. Chen, M. W. Wong, J. L. Andres, C. Gonzalez, M. Head-Gordon, E. S. Replogle, and J. A. Pople, *Gaussian, Inc.*, Pittsburgh PA, 1998.
15. C. L. Hussey and H. A. É'ye, *J. Electrochem. Soc.*, **131**, 1621 (1984).
16. S. Takahashi, N. Koura, S. Kohara, M. -L. Saboungi, and L. A. Curtiss, *Plasma & Ions*, **2**, 91 (1999).
17. G. Ling and N. Koura, *Denki Kagaku*, **65**, 149 (1997).
18. C. Rosenkilde, G. Voyiatzis, V. R. Jensen, M. Ystenes, and T. Ostvold, *Inorg. Chem.*, **34**, 4360 (1995).
19. W. Bues, F. Demiray, and W. Brockner, *Spectrochimica Acta*, **32A**, 1623 (1975).